JOURNAL OF SOLID STATE CHEMISTRY 106, 99–110 (1993)

Microstructural Investigation of Oxygen-Deficient $BaMnO_{3-y}$ Hexagonal Perovskites

J. M. GONZÁLEZ-CALBET,*† M. PARRAS,* J. M. ALONSO,*† AND M. VALLET-REGÍ†‡

*Departamento de Química Inorgánica, Facultad de Químicas, Universidad Complutense, 28040 Madrid, Spain; †Instituto de Magnetismo Aplicado, RENFE-UCM, Las Rozas, 28230 Madrid, Spain; and ‡Departamento de Química Inorgánica y Bioinorgánica, Facultad de Farmacia, Universidad Complutense, 28040 Madrid, Spain

Received December 4, 1992; accepted December 23, 1992

IN HONOR OF SIR JOHN MEURIG THOMAS ON HIS 60TH BIRTHDAY

The oxygen deficiency in the reduction process of the 2H $BaMnO_3$ hexagonal type leads to the introduction of $BaO_{2.5}$ cubic layers in the starting hexagonal close packing. A high-resolution electron microscopy study of the $BaMnO_{2.83}$ perovskite related oxide indicates that, as a function of the oxygen content and of the synthesis procedure, compositional variations in the $BaMnO_{3-y}$ system can be accommodated either by disordered intergrowths of both BaO_3 hexagonal $BaO_{2.5}$ cubic layers or by means of the formation of ordered hexagonal perovskite related phases.

Introduction

At the end of the 1970s and the beginning of the 1980s, a series of papers on chain silicates and zeolites by J. M. Thomas and coworkers ((*1–8*) and references therein) show that high-resolution electron microscopy (HREM), apart from strikingly confirming the validity of the X-ray based models giving structures averaged out over about 10^{18} unit cells, is able to solve either structural imperfections or superlattice structures that have been undetected by X-rays. In this extensive research on the internal structure of minerals and related solids, they proved that, with the arrival of a generation of transmission electron microscopes possessing a resolving power less than 0.3 nm point-to-point, it was possible to study local variations in the average structure which may represent regions of chemical constitution and activity different from those of the main structure.

The study of structural imperfections by means of a two-dimensional-projected image was crucial, in solid state chemistry, to modify the concept of nonstoichiometry. In fact, several authors (*9–11*) had demonstrated that some oxide systems previously considered classical solid solutions with randomly distributed point defects actually consisted of series of related crystal structures corresponding to specific compositions. The structures of these crystals correspond to superlattices derived by the ordering of point defects followed by their elimination by crystallographic shear. Since X-ray diffraction only detects long range periodicity, the observations were limited to rather large concentrations of solute or substantial deviations from stoichiometry where the periodic spacings were small and uniform. Now, it is well understood that compositional variations in metal oxides can be accommodated not only by random distribution of anionic vacancies or formation

0022-4596/93 $5.00

of ordered superstructures, if not by means of other more complex defects as, for instance, insertion of *CS* planes (*12, 13*), or disordered intergrowths of two or more basic structural motifs in various proportions (*14, 15*).

Probably, one of the structural families in which compositional variations have been more widely studied is that showing the perovskite-type structure. Perovskites are the earth's most abundant minerals and they are fascinating from a technological point of view because natural and synthetic perovskites exhibit a very wide array of properties. Regarding only their electrical properties, perovskites run the gamut, depending on the composition, from insulators to semiconductors, superionic conductors, metallike conductors, and high-temperature superconductors.

Due to this wide knowledge, a general consensus seems to exist about the trend of the defect chemistry of perovskite related oxides. However, despite this interest, compositional variations are only well known in AMO_{3-y} perovskite related materials when the AO_3 layer stacking is cubic, three cubic layers being needed to describe the unit cell following a ...ccc... sequence. Among all these materials, ferrites are the most extensively studied phases because Mössbauer spectroscopy is used to determine both the environment and oxidation state of the iron atoms. Thus, both octahedral and tetrahedral sites can coexist within the same framework (*16, 17*) in the AMO_3–$AMO_{2.5}$ range. Between the ordered perovskite-related phases described up to now showing cubic packing, square pyramidal coordination has only been detected when Ba atoms are occupying the *A* sublattice (*18–20*).

A different location of oxygen vacancies has been observed in the $CaMnO_{3-y}$ system due to the presence of square pyramids for the Jahn–Teller Mn^{3+} ion (*21–24*). In a very smart paper, Reller *et al.* (*23*) stated that the unit cells of fully oxygenated and oxygen-deficient $CaMnO_{3-x}$ compounds are all related if they are viewed as superlattices of the parent perovskite derived from a rotation angle in the metal–oxygen planes.

Compositional variations have been less studied in hexagonal perovskites. For a hexagonal close packing only two hexagonal layers are necessary to complete the unit cell in the ...hhh... stacking sequence (2H structural type) (*25*). Between both cubic and hexagonal terms, several unique structure types theoretically can be generated (*26*). Electron diffraction and microscopy studies performed on the $BaFeO_{3-y}$ system (*27, 28*) indicate that only two hexagonal phases appear: a 12R type, formed by octahedra sharing faces linked by octahedra sharing vertices, giving a stacking sequence $(hhcc)_3$ (*29*), and a 6H type, isostructural with $BaTiO_3$ (*30*).

Once again, the situation is different when Mn is occupying the *M* sites of the perovskite lattice. Negas and Roth (*31*) have shown by means of X-ray diffraction that $BaMnO_3$ adopts the 2H structural type, a series of different hexagonal phases existing in the anion deficient $BaMnO_{3-y}$ ($0 \leq y \leq 0.25$) system: a rhombohedral 15-layer form and hexagonal 8H, 6H, 10H and 4H types. An electron microscopy study (*32*) shows that 2H $BaMnO_3$ is transformed under the electron beam to both 6H and 10H types. However, no correlation has been established between the oxygen content and the different structural types. In order to study the accommodation of the anionic vacancies in this system, we have undertaken an investigation, by means of selected area electron diffraction (SAED) and HREM, of $BaMnO_{3-y}$ materials with accurate control of oxygen stoichiometry. We describe in this paper the 6H $BaMnO_{2.83}$ phase and its comparison with 6H $BaFeO_{3-y}$.

2. Synthesis and Microstructural Characterization of 6H $BaMnO_{2.83}$

In order to synthesize a 6H $BaMnO_{3-y}$ type, a similar procedure to that described by Negas and Roth was followed (*31*). First,

$BaMnO_3$ (2H type) was obtained by solid-state reaction from stoichiometric amounts of $BaCO_3$ and $MnCO_3$.

Both powder X-ray and electron diffraction patterns of the $BaMnO_3$ sample so obtained can be indexed on the basis of a 2H structural type unit cell of parameters a = 0.57 and c = 0.48 nm (*33*).

Then, the sample was heated at 1300°C in air for 72 hr and annealed under vacuum at 1040°C for 24 hr. The corresponding powder X-ray diffraction pattern, shown in Fig. 1, can be indexed on the basis of the 6H hexagonal type (a = 0.57, c = 1.4 nm).

The oxygen content was thermogravimetrically determined by reduction in dry hydrogen following the procedure described in Ref. (*34*). From the weight loss, an average composition $BaMnO_{2.83}$, i.e., $Ba_6Mn_6O_{17}$, is obtained.

The electron diffraction and microscopy study shows, however, a more complex situation. Figure 2 shows the SAED pattern (Fig. 2a) and the corresponding high-resolution electron micrograph (Fig. 2b), performed on a JEOL 4000EX electron microscope, along the [010] zone axis. Streaking along the c^*-axis, suggesting the existence of structural disorder, is clearly reflected in the image, where a disordered intergrowth of fringes with different d-spacings can be seen following the c-axis.

Taking into account that the distance between black dots is ~0.23 nm along the c-axis, which correspond to the distance of two adjacent BaO_3 layers, the (d-spacing/0.23) ratio allows us to obtain the number of BaO_3 layers (n) constituting each one of the intergrowing structural types. Moreover, the stacking sequence characteristic of every structural type can be deduced from the different contrast observed in the high-resolution electron micrograph. According to that, the structure image (Fig. 2b) can be interpreted in the following way:

—Areas showing d-spacing = 0.48 nm (n = 2), correspond to a stacking sequence ...hhh... characteristic of the 2H structural type.

—d-spacing = 1.4 nm (n = 6): ...chchhhc... stacking sequence corresponding to the 6H type (*31*).

For a d-spacing = 1.9 nm (n = 8), two different stacking sequences can be observed: (i) ...$(chhh)_2$... corresponding to the 8H type described by Negas and Roth (*31*) see also (*35*); (ii) ...chhhhhchc... (marked 8H′ in the image) which has also been found as a stacking fault in $BaMn_{0.767}Fe_{0.233}O_{2.87}$ (*36*).

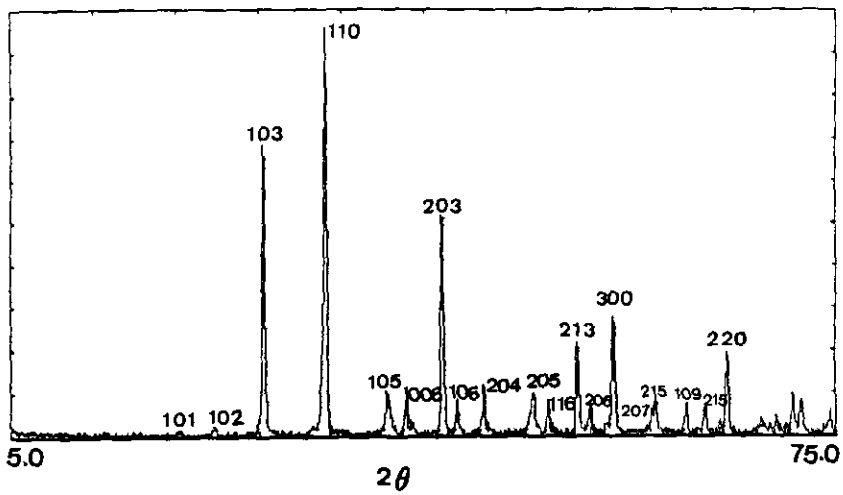

FIG. 1. Powder X-ray diffraction pattern of 6H $BaMnO_{2.83}$.

Image calculations of the different structural models were performed by using the multislice method (*37*), under the following image conditions: sample thickness (t) between 3 and 6 nm; $\Delta f \simeq -60$ and -70 nm; $C_s = 1.0$ nm; $C_c \simeq 1.7$ nm; beam divergence angle $= 0.8 \times 10^{-3}$ rad, and accelerating voltage = 400 kV. Figures 3–6 show the calculated images along [010] of the 2H, 6H, 8H, and 8H′ structural types, respectively. According to the image contrast observed, the 8H′ polytype shows a chhhhhchc stacking sequence, |211|112| Zhdanov notation, space group $P\bar{6}m2$. A detailed discussion of the stacking of close-packed units, generated symmetry, and descriptive Zhdanov notation is provided in the "International Tables for X-ray Crystallography" (*38*). By supposing an ideal 8H′ layer sequence with $P\bar{6}m2$ symmetry, the corresponding atomic positions are: 1 Ba in (a); 1 Ba in (f); 2 Ba in (h), $z \simeq 1/8$, 2 Ba in (h), $z \simeq 3/8$; 2 Ba in (i), $z \simeq 2/8$; 2 Mn in (g), $z \simeq 3/16$; 2 Mn in (g), $z \simeq 5/16$; 2 Mn in (g), $z \simeq 7/16$; 2 Mn in (i), $z \simeq 1/16$; 6 O in (n), $x \simeq 1/6$, $z \simeq 1/8$; 6 O in (n), $x \simeq 5/6$, $z \simeq 2/8$; 6 O in (n), $x \simeq 5/6$, $z \simeq 3/8$; 3 O in (k), $x \simeq 1/6$; and 3 O in (j), $x \simeq 1/2$.

The corresponding structural projected models along [010] are also shown. The best fit seems to be obtained, in all cases, for $t = 4$ and $\Delta = -60$ nm. It is worth mentioning that in the simulated images all the white dots show the same intensity, while in the experimental micrograph some of the cubic layers show a different intensity. In fact, this is because image calculations have been carried out considering a BaO_3 stoichiometry in every layer on the basis of an ideal sequence of n-layers ($n = 2$, 6, and 8, respectively). This introduces a change with respect to the true stoichiometry of the 6H, 8H and 8H′ structural types, since all of them must show oxygen deficiency.

At this point, it is worth recalling that the powder X-ray diffraction pattern only shows reflections characteristic of the 6H structural type. In fact, this type appears frequently ordered along several unit cells as observed in another area of the same crystal (Fig. 7). On the contrary, the other hexagonal-types only intergrow in a disordered way along the c-axis, at the level of one or two unit cells (see Fig. 2b).

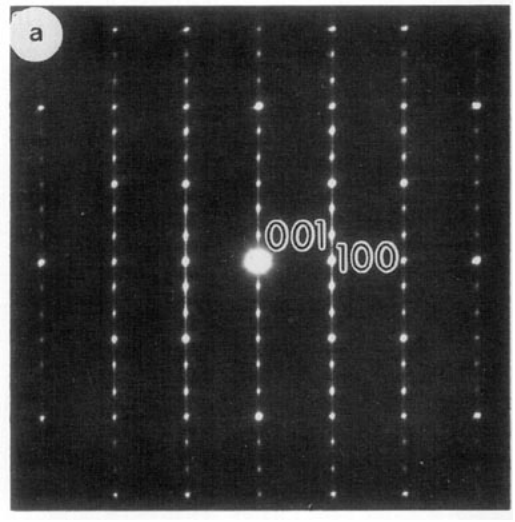

FIG. 2. (a) SAED of $BaMnO_{2.83}$ along [010]. (b) Corresponding HREM image. A disordered intergrowth of 2H, 6H, 8H, and 8H′ types is observed. Intersecting blocks (chc) are marked.

The origin of such a disorder, probably resides in the nature of the precursor obtained at 1300°C in air for 72 hr. Effectively, although the powder X-ray diffraction pattern corresponds to the 15R structural type (*31*), the SAED pattern along the [010] zone axis (Fig. 8) shows a highly disordered material along the c^*-axis. This intermediate step was avoided to obtain an ordered 6H phase. So, the well ordered 2H $BaMnO_3$ material was directly annealed under vacuum at 1040°C for 24 hr. The material so obtained shows identical $BaMnO_{2.83}$ composition but with an ordered situation as observed in both SAED pattern and corresponding micrograph along [010] (Fig. 9).

Since 2H $BaMnO_3$ is only formed by BaO_3 hexagonal layers (see structural model in Fig. 3) and the reduction process leads to the formation of cubic layers, we can assume that oxygen vacancies are accommodated in these layers. Moreover, taking into

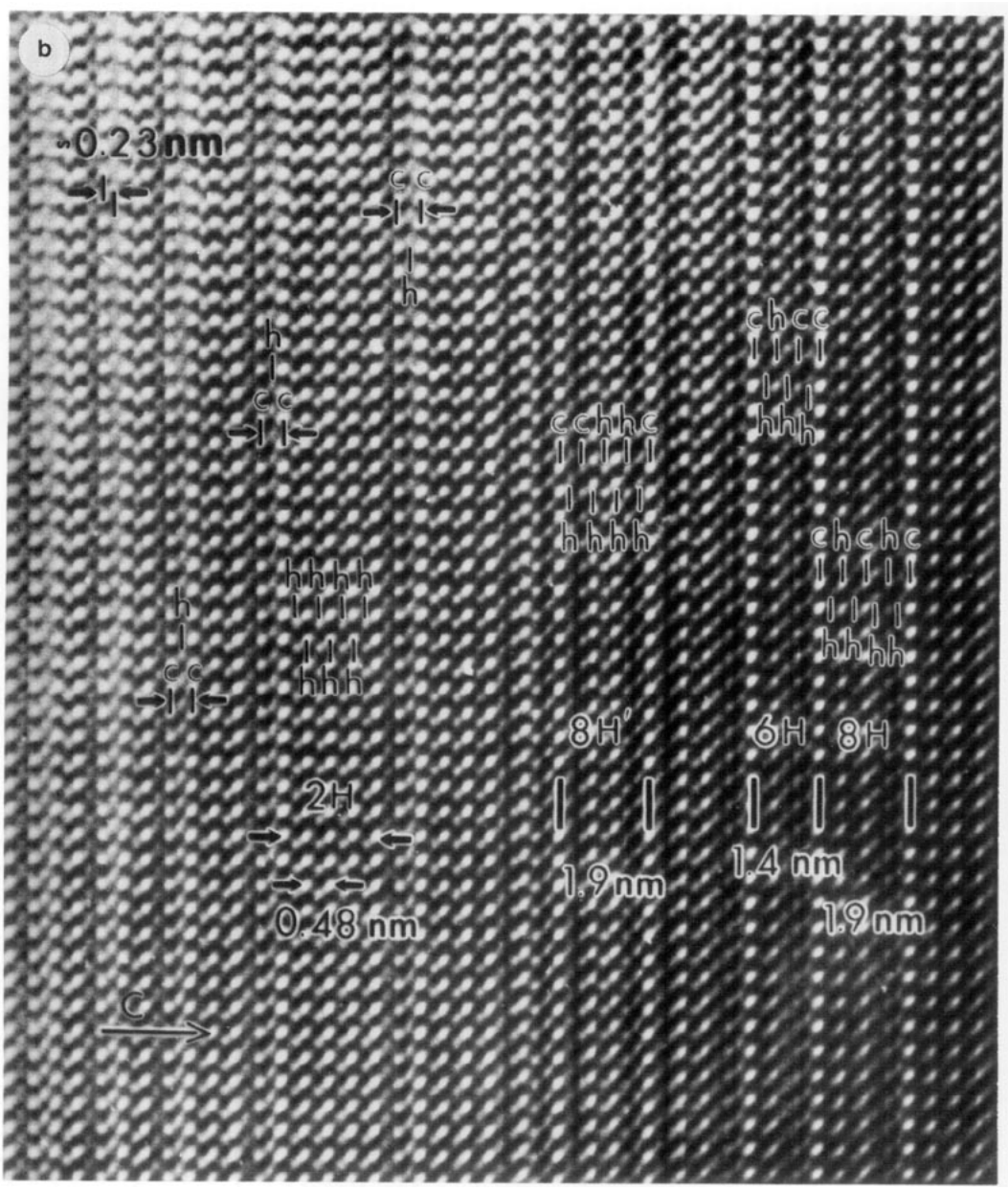

FIG. 2.—*Continued*

account the strong tendency of Mn^{3+} to be stabilized in square pyramidal coordination in perovskite-related oxides (*21*), only one oxygen in every six can be removed in each cubic layer ($BaO_{2.5}$ composition). Since the stacking sequence of the 6H structural type is constituted by two cubic and four hexagonal layers, the ideal composition for such a structural type would be $Ba_6Mn_6O_{17}$ (2 $BaO_{2.5}$ + 4 BaO_3), i.e., $BaMnO_{2.83}$ per unit formula, in agreement with the experimental composition.

On the basis of these ideas, the ideal composition of the different hexagonal types can

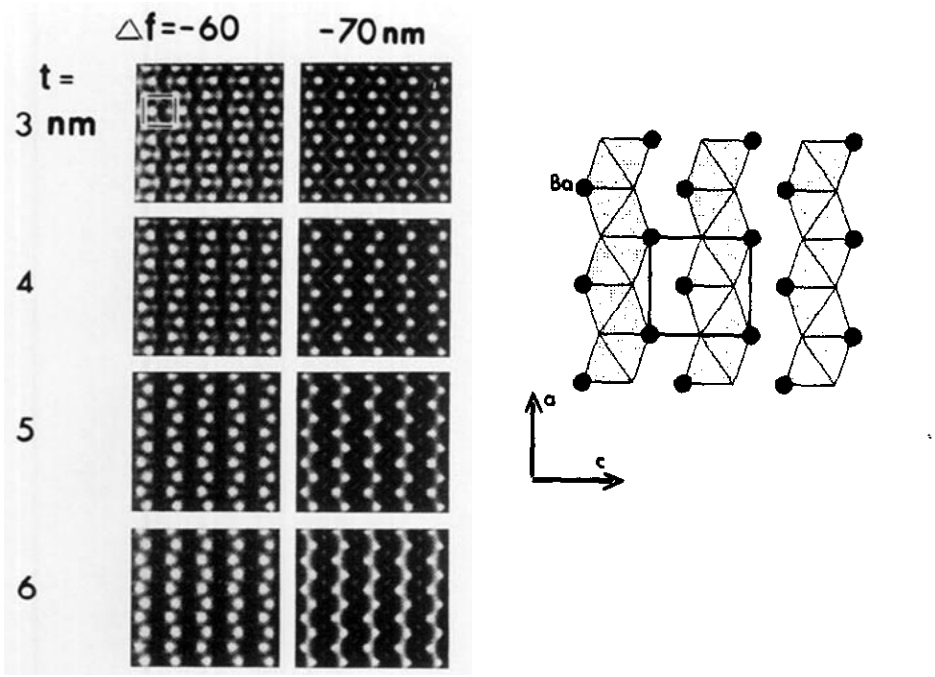

FIG. 3. Calculated image and structural model projection corresponding to the 2H structural type along [010] on the basis of an ideal 2H layer sequence with $P6_3mc$ symmetry. The unit cell is outlined.

be calculated from the stacking sequence they show. Thus, in the case of both 8H and 8H′ polytypes, the ideal composition would be $Ba_8Mn_8O_{23}$, i.e., $BaMnO_{2.87}$. Coming back to the high resolution image shown in Fig. 2b, three phases with ideal composition $BaMnO_3$ ($n = 2$), $BaMnO_{2.87}$ ($n = 8$), and $BaMnO_{2.83}$ ($n = 6$) were identified. This obviously gives an average composition higher than the experimental one ($BaMnO_{2.83}$). However, the structural intergrowth takes place, in many cases, by means of a (chc) block (as marked in Fig. 2b) which should have a $BaO_{2.67}$ composition.

On the basis of the location of the oxygen defect, the image calculations have been reconsidered by assuming that the average composition of every cubic layer is $BaO_{2.5}$. Then, one oxygen in every six was removed per cubic layer, with random distribution of the oxygen vacancies. This modification does not originate any change in the contrast observed in the calculated images. However, such a structural change must be accompanied of a displacement of the heaviest atoms which can be responsible for the different changes observed in the structure image. In order to solve this problem, neutron diffraction studies are in progress.

3. Discussion

Since X-ray diffraction only detects long-range periodicity, electron diffraction and lattice imaging are necessary to follow the clustering of anionic vacancies when the oxygen deficiency increases from the 2H structural type to the different hexagonal types existing in the $BaMnO_{3-y}$ system. Only in the perovskite hexagonal systems studied in such a way it has been possible to determine the stability range of the different structural types.

Thus, two different hexagonal types have been described in the $BaFeO_{3-y}$ ($0 < y < 0.5$) perovskite-related system, according to

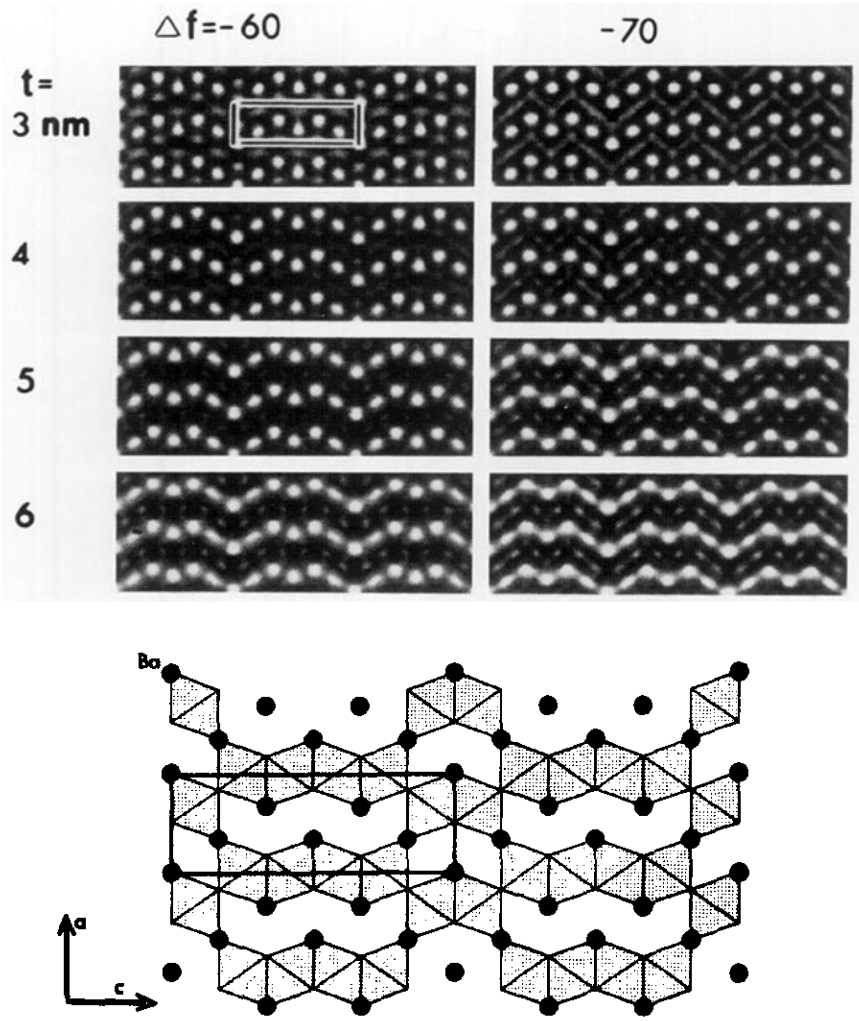

FIG. 4. Calculated image and structural model projection corresponding to the 6H structural type along [010] on the basis of an ideal 6H layer sequence with $P6m2$ symmetry. The unit cell is outlined.

powder X-ray diffraction patterns: A 12R structural type in the composition range $BaFeO_{2.93}$-$BaFeO_{2.87}$ (*29*) and a 6H type between $BaFeO_{2.80}$ and $BaFeO_{2.65}$ (*28*). It is worth mentioning that the 6H hexagonal type in $BaFeO_{3-y}$ shows a ...hcchcc... layer stacking sequence along the *c*-axis. Note that although the number of layers per unit cell is, as in $BaMnO_{3-y}$, six, the layer stacking is somewhat different.

Electron diffraction and microscopy studies in the 6H $BaFeO_{3-y}$ compositional range show two different situations: between $BaFeO_{2.80}$ and $BaFeO_{2.75}$, both electron diffraction patterns and corresponding micrographs only show this structural type. However, for lower amounts of Fe^{4+}, stacking faults along the c-axis are observed, which correspond to a ...ccc... stacking sequence (see Figs. 5 and 6 of Ref. (*28*)).

Neutron diffraction studies performed by Jacobson (*39*) on a $BaFeO_{2.75}$ 6H-type lead to $BaO_{2.875}$ composition for every cubic layer and $BaO_{2.5}$ composition for hexagonal

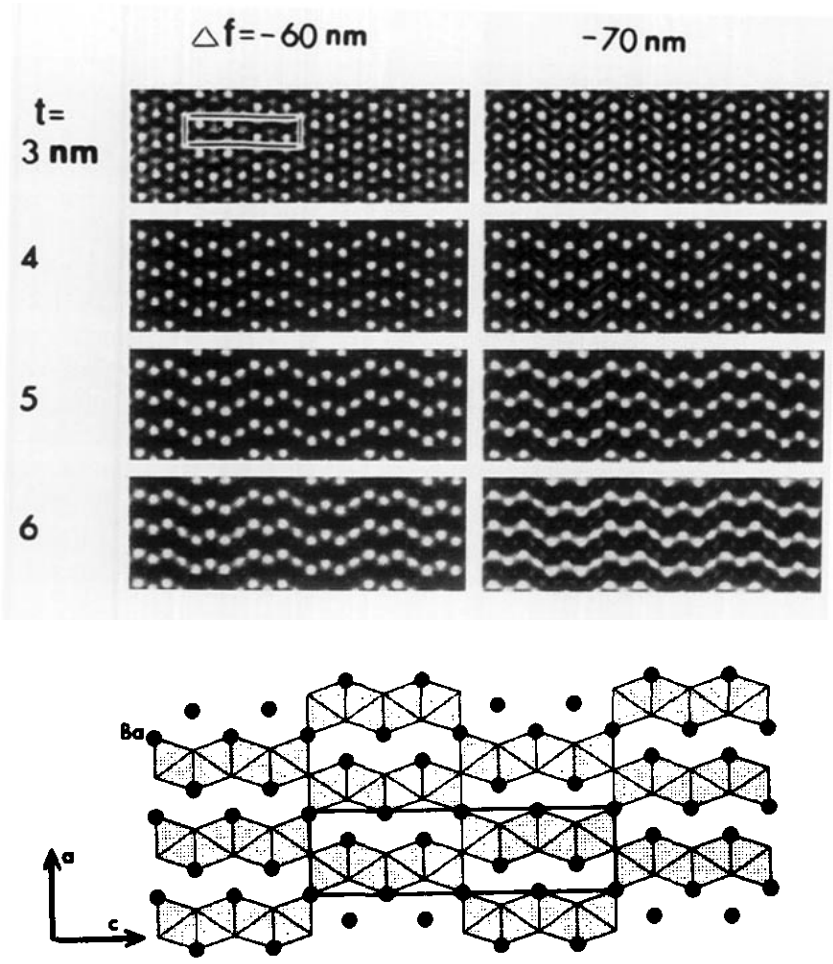

FIG. 5. Calculated image and structural model projection corresponding to the 8H structural type along [010] on the basis of an ideal 8H layer sequence with $P63/mmc$ symmetry. The unit cell is outlined.

layers. However, since electron diffraction studies indicate that this system allows compositional variations along the same structural type, it seems obvious that the composition in the stacking layers cannot remain fixed.

This behavior is clearly different of that shown by the $BaMnO_{3-y}$ system. Compositional variations in $BaMnO_{3-y}$ can be accommodated either by disordered intergrowths of hexagonal types or by means of the formation of ordered phases, as in the case of $BaMnO_{2.83}$. In any case, the concentration of anionic vacancies seems to determine the number of $BaO_{2.5}$ cubic layers and, therefore, the resulting structural type. On the contrary, the $BaFeO_{3-y}$ system seems to admit the presence of oxygen vacancies in both hexagonal and cubic layers, which facilitates the existence of a given hexagonal type along a certain compositional range. However, the fact that in the $BaMnO_{3-y}$ system both hexagonal and cubic layers have a fixed composition, BaO_3 and $BaO_{2.5}$, respectively, prevents compositional variations keeping the same structural type. Moreover, local compositional variations in this system lead to the formation of a differ-

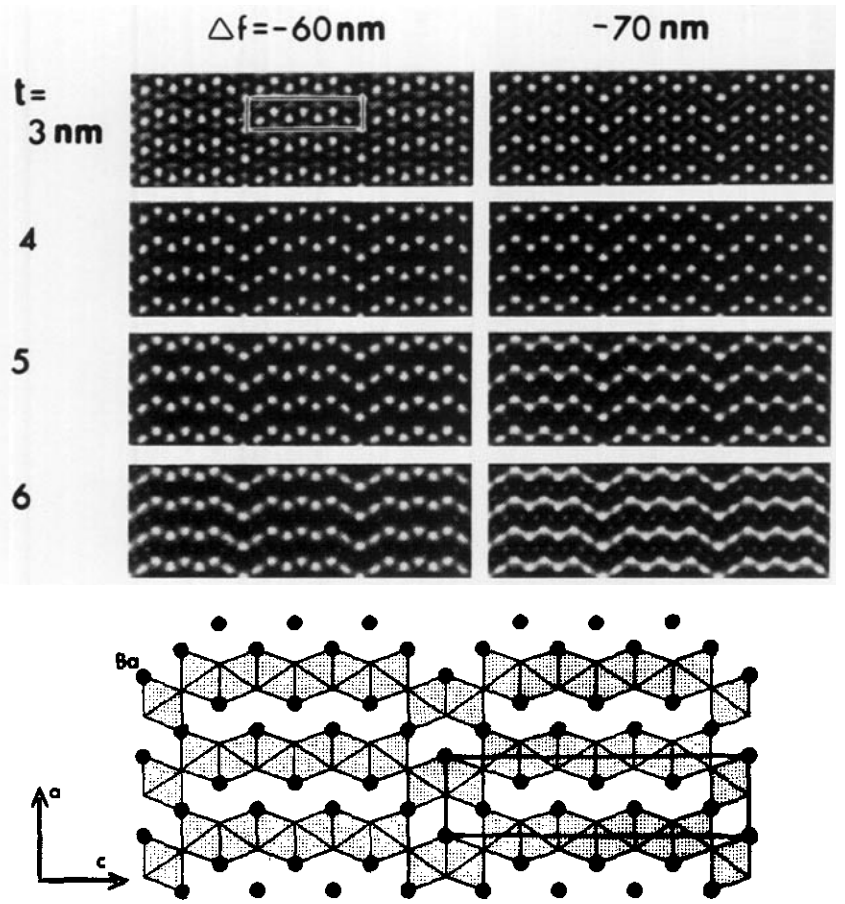

FIG. 6. Calculated image and structural model projection corresponding to the 8H′ structural type along [010] on the basis of an ideal 8H′ layer sequence with $P6_3m2$ symmetry. The unit cell is outlined.

ent structural type, even at the unit cell level. Therefore, it seems that every structural type in the $BaMnO_{3-y}$ system requires a defined composition.

However, two different situations have been encountered for the same $BaMnO_{2.83}$ composition. This indicates that having a defined composition is a necessary but not sufficient condition. When $BaMnO_3$ is reduced, Mn can accommodate the anion loss by assuming a permissible lower coordination number. As we mentioned above, an ordered 6H phase was only obtained by starting from a well ordered 2H $BaMnO_3$ material. Nevertheless, compositional variations in $BaMnO_{3-y}$ can be accommodated by disordered intergrowths when precursor materials are disordered. It is well known that the synthesis of nonstoichiometric compounds often depends on the structure of the starting material since this feature can have a large influence on the material's reactivity, as observed in the oxide shear phases of Group 5 and 6 transition metals. Therefore, the attainment of an ordered phase seems to be dependent on both the starting material and the final composition. In fact, Negas and Roth (*31*), by means of X-ray diffraction, established that 15R, 8H, 6H, 10H, and 4H structural types allow compo-

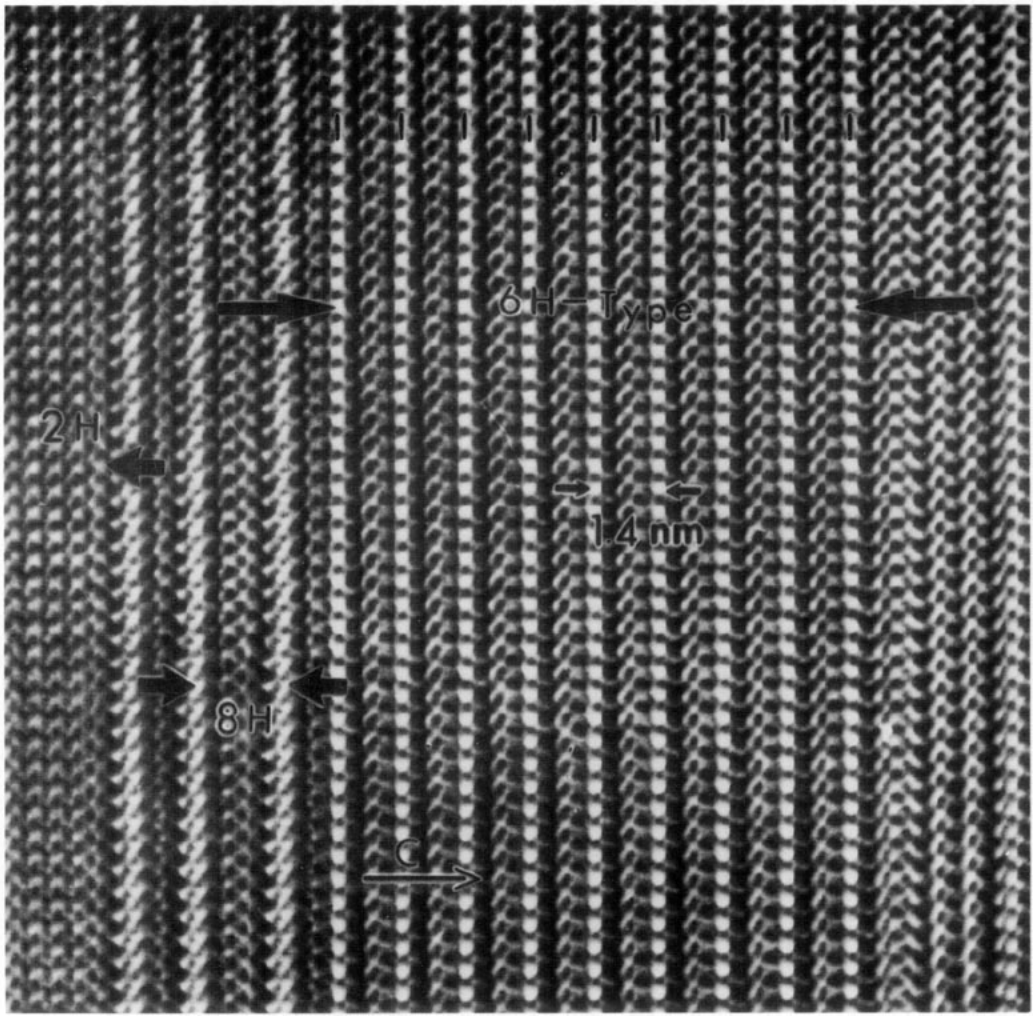

FIG. 7. HREM image of another area of the crystal shown in Fig. 2b. A rather long ordered 6H type (8 unit cells) is observed.

sitional variations in a narrow range. None of the compositions determined by these authors is in agreement with the theoretical values deduced from the corresponding structural type by assuming BaO_3 and $BaO_{2.5}$ compositions for hexagonal and cubic layers, respectively: $BaMnO_{2.90}$ (15R), $BaMnO_{2.87}$(8H), $BaMnO_{2.83}$(6H), $BaMnO_{2.80}$ (10H), and $BaMnO_{2.75}$ (4H). Moreover, in most cases, these authors start from disordered materials, as confirmed by Fig. 8. According to our ideas, the microstructure of these materials should be constituted by disordered intergrowths of several hexagonal types, although the average structure corresponds to a given type. In order to complete the study of compositional variations in $BaMnO_{3-y}$, an electron microscopy study of samples with accurate control of oxygen stoichiometry is in progress.

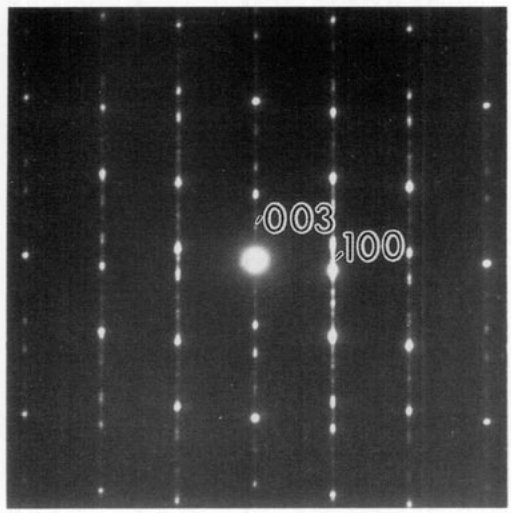

FIG. 8. SAED pattern of the 15H type showing streaking along the c^*-axis, indicative of a highly disordered material.

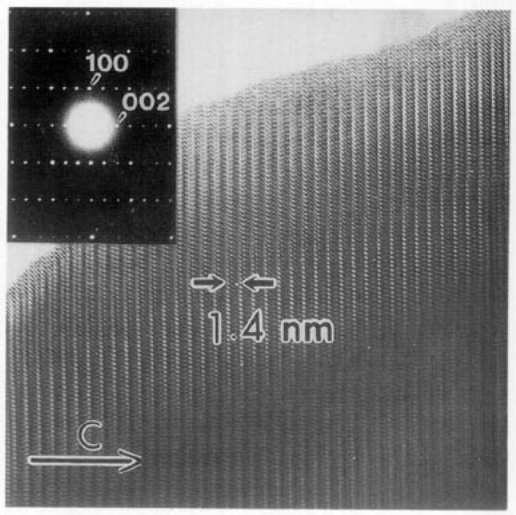

FIG. 9. Electron micrograph and corresponding SAED pattern of 6H $BaMnO_{2.83}$ (ordered phase) along the [010] zone axis.

Acknowledgments

We acknowledge the financial support of C.I.C.Y.T. (Spain) through Research Projects MAT 90-0858-C02-02 and MAT 91-0331. We are also grateful to Mr. A. García, Mr. E. Baldonedo, and Mr. P. Robredo for valuable technical assistance.

References

1. J. M. THOMAS AND D. A. JEFFERSON, *Endeavour N. S.* **2,** 127 (1978).
2. J. M. THOMAS, *New Sci.* **88,** 580 (1980).
3. M. BEER, R. W. CARPENTER, L. EYRING, C. E. LYMAN, AND J. M. THOMAS, *Chem. Eng. News* **59,** 40 (1981).
4. D. A. JEFFERSON, J. M. THOMAS, AND R. F. EGERTON, *Chem. Br.* **17,** 514 (1981).
5. J. M. THOMAS, S. RAMDAS, G. R. MILLWARD, J. KLINOWSKI, M. AUDIER, J. M. GONZÁLEZ-CALBET, AND C. A. FYFE, *J. Solid State Chem.* **45,** 368 (1982).
6. J. M. THOMAS, *Ultramicroscopy* **8,** 13 (1982).
7. J. M. THOMAS, D. A. JEFFERSON, AND G. R. MILLWARD, *J. Microsc. Spectrosc. Electron.* **7,** 315 (1982).
8. G. R. MILLWARD, S. RAMDAS, AND J. M. THOMAS, *Proc. R. Soc. London Ser. A* **399,** 57 (1985).
9. S. ANDERSSON, *Bull. Soc. Fr. Mineral. Cristallogr.* **90,** 522 (1967).
10. D. A. WADSLEY, *in* "Nonstoichiometric Compounds" (L. Mandelcorn, Ed.), Chap. 3, p. 135, Academic Press, New York (1964).
11. J. S. ANDERSON, "Shear Structures and Nonstoichiometry" *in* "Surface and Defect Properties of Solids" (J. M. Thomas and M. W. Roberts, Eds.), The Chemical Society, London (1972).
12. J. M. GONZÁLEZ-CALBET, D. A. JEFFERSON, J. DRENNAN, AND P. C. SPURDENS, *Mater. Res. Bull.* **16,** 1107 (1981).
13. L. C. OTERO-DÍAZ AND B. HYDE, *Acta Crystallogr. Sect. B* **40,** 237 (1984).
14. J. M. GONZÁLEZ-CALBET, M. VALLET-REGÍ, M. A. ALARIO-FRANCO, AND J. C. GRENIER, *Mat. Res. Bull.* **18,** 285 (1983).
15. M. VALLET-REGÍ, J. M. GONZÁLEZ-CALBET, M. A. ALARIO-FRANCO, J. C. GRENIER, AND P. HAGENMULLER, *J. Solid State Chem.* **55,** 251 (1984).
16. J. C. GRENIER, M. POUCHARD, AND P. HAGENMULLER, *Struct. Bonding* **47,** 1 (1981).
17. J. M. GONZÁLEZ-CALBET AND M. VALLET-REGÍ, *J. Solid State Chem.* **68,** 266 (1987).
18. M. PARRAS, L. FOURNES, J. C. GRENIER, M. POUCHARD, M. VALLET-REGÍ, J. M. GONZÁLEZ-CALBET, AND P. HAGENMULLER, *J. Solid State Chem.* **88,** 261 (1990); X. D. ZOU, S. HOVMÖLLER, M. PARRAS, M. VALLET-REGÍ AND J. M. GONZÁLEZ-CALBET, *Acta Crystallogr., Sect. A* **49,** 27 (1993).
19. Q. HUANG, P. KAREN, V. L. KAREN, A. KJEKSHUS, J. W. LYNN, A. D. MIGHELL, N. ROSOV, AND A. SANTORO, *Phys. Rev. B* **45,** 9611 (1992).

20. E. García-González, M. Parras, J. M. González-Calbet, and M. Vallet-Regí, *J. Solid State Chem.* **104,** 232 (1993).
21. K. R. Poeppelmeier, M. E. Leonoewicz, and J. M. Longo, *J. Solid State Chem.* **44,** 89 (1982).
22. K. R. Poeppelmeier, M. E. Leonoewicz, J. C. Scanlon, and J. M. Longo, *J. Solid State Chem.* **45,** 71 (1982).
23. A. Reller, J. M. Thomas, D. A. Jefferson, and M. K. Uppal, *Proc. R. Soc. London Ser. A* **394,** 223 (1984).
24. C. C. K. Chiang and K. R. Poeppelmeier, *Mater. Lett.* **12,** 102 (1991).
25. J. J. Lander, *Acta Crystallogr.* **4,** 148 (1951).
26. L. Katz and R. Ward, *Inorg. Chem.* **3(2),** 205 (1964).
27. J. C. Grenier, A. Wattiaux, M. Pouchard, P. Hagenmuller, M. Parras, M. Vallet-Regí, J. M. González-Calbet, and M. A. Alario-Franco, *J. Solid State Chem.* **80,** 6 (1989).
28. M. Parras, M. Vallet-Regí, J. M. González-Calbet, and J. C. Grenier, *J. Solid State Chem.* **83,** 121 (1989).
29. M. Parras, M. Vallet-Regí, J. M. González-Calbet, J. C. Grenier, P. Hagenmuller, and J. Rodríguez-Carvajal, *Eur. J. Solid State Inorg. Chem.* **26,** 299 (1989).
30. R. D. Burbank and H. T. Evans, *Acta Crystallogr.* **1,** 330 (1948).
31. T. Negas and R. S. Roth, *J. Solid State Chem.* **3,** 323 (1971).
32. H. Shibahara and H. Hashimoto, *J. Cryst. Growth* **65,** 683 (1983).
33. A. Hardy, *Acta Crystallogr.* **15,** 179 (1962).
34. A. Caneiro, M. Vallet-Regí, J. Ramírez, P. Crespo, and J. M. González-Calbet, *Solid State Commun.* **82(2),** 95 (1992).
35. A. D. Pottot, L. Chamberland, and L. Katz, *J. Solid State Chem.* **8,** 234 (1973).
36. V. Caignaert, M. Hervieu, B. Domenges, N. Nguyen, J. Pannetier, and B. Raveau, *J. Solid State Chem.* **73,** 107 (1988).
37. NCEMSS Programm, National Center for Electron Microscopy, Materials and Chemical Science Division, Lawrence Berkeley Laboratory, University of California, Berkeley, California (1989).
38. International Tables for X-ray Crystallography," Vol. II, p. 342, Kynoch Press, Birmingham (1959).
39. A. Jacobson, *Acta Crystallogr. Sect. B* **32,** 1087 (1976).